Inorganic Chemistry

Article

pubs.acs.org/IC

Magnetooptical and Structural Investigations of Five Dimeric Cobalt(II) Complexes Mimicking Metalloenzyme Active Sites

Z. Tomkowicz,*[,†,‡] S. Ostrovsky,[†,§] S. Foro,[⊥] V. Calvo-Perez,[¶] and W. Haase*[,†]

[†]Eduard-Zintl-Institute of Inorganic and Physical Chemistry, Darmstadt University of Technology, Petersenstrasse 20, 64287 Darmstadt, Germany

[‡]Institute of Physics, Jagiellonian University, Reymonta 4, 30-059 Kraków, Poland

[§]Institute of Applied Physics, Academy of Sciences of Moldova, Academy str. 5, MD-2028 Chisinau, Moldova

[⊥]Clemens-Schoepf-Institute of Organic Chemistry and Biochemistry, Darmstadt University of Technology, Petersenstrasse 23, 64287 Darmstadt, Germany

[¶]Facultad Ciencias Químicas y Farmacéuticas, Universidad de Chile, Casilla 233, Santiago, Chile

Supporting Information

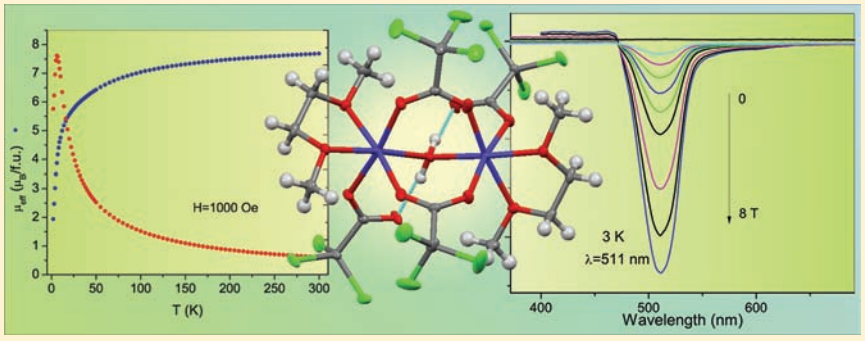

ABSTRACT: Four novel cobalt(II) complexes mimicking metalloenzyme active sites, novel $C_{14}H_{22}Cl_{12}Co_2O_{13}\cdot 2C_3H_8O$ (**1**), $C_{28}H_{36}Cl_{24}Co_4O_{28}\cdot 4C_4H_8O_2$ (**2**), $C_{16}H_{22}Cl_{12}Co_2O_{13}\cdot C_2HCl_3O_2$ (**3**), $C_{16}H_{22}Cl_{12}Co_2O_{13}$ (**4**), and one known $C_{40}H_{78}Cl_8Co_2O_{17}$ (**5**) are composed of the same core of two high-spin cobalt(II) centers triply bridged by water and two trichloroacetato (**1**−**4**) or two pivalate (**5**) groups but differ in terminal ligands. The crystal structures of new compounds **1**−**4** belong to the space groups $P\bar{1}$, $P2_1/c$, $P\bar{1}$, and *Pbcn*, respectively. All five investigated complexes contain Co atoms in distorted octahedral coordination. The complexes were characterized by magnetic susceptibility and magnetization measurements and by variable-temperature variable-field magnetic circular dichroism spectroscopy. Experimental data were analyzed in the frame of the theoretical model, which includes an unquenched orbital moment of the Co^{II} ions. All investigated compounds are antiferromagnetically coupled with exchange constants in the range −1.5 to −2.1 cm^{-1}. However, there is a significant difference between the crystal-field-splitting parameters.

1. INTRODUCTION

Carboxylato groups as bridging ligands are essential parts of the catalytic site of a family of metalloproteins from archaeal peptidases, glycerophosphodiesterase, and phosphotriesterase to methionine and leucine aminopeptidases.[1] The large versatility of structures with carboxylate ligands is in favor of using them as active-site models, mimicking the native ones, for new artificial metalloenzymes. The important research task is to capture the structural and electronic parameters, which would be optimal for biocatalytic processes. More importantly, the chemical models may provide information about the Michaelis complex, which is not always accessible via X-ray diffraction (XRD) because this method requires the solid phase or at least a frozen form of the protein. Hence, the catalytic mechanism cannot be described using exclusively protein XRD.[2] Therefore, other tools such as variable-temperature variable-field magnetic circular dichroism (VTVH-MCD) spectroscopy have been used by several research groups for monitoring high-spin transition-metal ions in their chemical environment within the metalloenzymes[3] and to model the coordination mode of these metals.[4] Both VTVH-MCD and high-field electron paramagnetic resonance (HFEPR) spectroscopy were used to monitor slight distortions of a coordinated transition-metal center of some model cobalt(II) complexes.[5] In parallel, also magnetic measurements may be used, providing information on magnetic coupling and crystal-field splitting.

In this work, we studied four new dimeric cobalt(II) complexes by using XRD and magnetic measurements completed by VTVH-MCD. The core of these complexes is

Received: November 29, 2011
Published: May 23, 2012

   dx.doi.org/10.1021/ic202529p | *Inorg. Chem.* 2012, 51, 6046−6055

$Co_2(\mu\text{-}H_2O)(\mu\text{-}OOC\text{-}R)_2$ (R = CCl_3), with two Co atoms in distorted octahedral positions. Such complexes are good models for the active site of some metalloenzymes. The core of similar topology occurs in urease but with Ni atoms. Ubiquitous methionine aminopeptidase contains Co atoms, one of them occupies the six-coordinated position and the second one is in the five-coordinated position. Although our knowledge about the existence of native cobalt metalloenzymes is limited, the Co^{II} ion has a remarkable advantage in replacing the native metal ions in metalloenzymes, retaining their activity and the active-site structure (e.g., Co for Zn in carbonic anhydrase,[6] alcohol dehydrogenase,[7] and insulin hexamer[8] or Co^{II} for Cu^{II} in hemocyanin[9,10]). It then becomes an excellent spectroscopic probe useful for the study of electronic and catalytic properties.

The $Co_2(\mu\text{-}H_2O)(\mu\text{-}OOC\text{-}R)_2$ core models for some metalloenzymes (but with mixed five- and six-coordinated Co atoms) were the object of intensive VTVH-MCD studies; see ref 11 and references cited therein. Also, some $M_2(\mu\text{-}OOC\text{-}R)_3L$ complexes (L is a terminal ligand) were magnetically studied and examined as models for the catalase activity in a *N*,*N*-dimethylformamide solution, where M, among others, was Co^{II} with 5-fold coordination.[12] The structural details of $Co_2(\mu\text{-}H_2O)(\mu\text{-}OOC\text{-}R)_2$ core models, such as the Co···Co distance, the Co−OH_2−Co angle, and, more importantly, the nature of the bridging O atom (μ-aquo or μ-hydroxo) are crucial to explaining the magnetic properties, as shown by Turpeinen et al.,[13] for a series of dicobalt μ-aquotrichloroacetato complexes. Larrabee et al.[11] found recently that protonation of the bridging OH group strongly affects the magnetic properties of the dicobalt(II) carboxylato center in a related $Co_2(\mu\text{-}H_2O)(\mu\text{-}OOC\text{-}R)_2$ core model. This observation obtained by MCD allows one to propose the mechanistic details, rarely detectable by protein XRD.[2]

It should be mentioned here that $Co_2(\mu\text{-}H_2O)(\mu\text{-}OOC\text{-}R)_2$ core groups have been found in extended solids, where the carboxylato group is substituted by benzenetetracarboxylic or phenylenediacetic groups.[14] These 3D solids present some moderate intrachain ferromagnetic exchange coupling (J_{ex} = +5.4 to +2.1 cm^{-1}) occurring at Co···Co distances comparable to those found in the previously mentioned enzymes. This is an interesting circumstance in light of the design of new promising materials, as single-chain magnets, that could find applications in magnetic devices.[15]

Recently, we have reported on a trimeric chain compound composed of $Co^{II}(\mu\text{-}H_2O)(\mu\text{-}OOC\text{-}CF_3)_2$ units,[16] where the bridging water and two trifluoroacetates mediate in very weak antiferromagnetic exchange interactions, so that each octahedrally coordinated Co^{II} behaves practically as an isolated high-spin center with large L−S coupling. The present work is a continuation of this study. The high-spin dinuclear complexes that were synthesized have the general formula $Co_2(\mu\text{-}H_2O)(\mu\text{-}OOC\text{-}R)_2(OOC\text{-}R)_2(H_2O)_2L_2$ (R = CCl_3) with the central core dicobalt(II) μ-aquo di-μ-carboxylate. These compounds were obtained by crystallization in different solvents: isopropyl alcohol (IPA), 1,4-dioxane, tetrahydrofuran (THF), or 1,2-dimethoxyethane (glyme). Their abbreviated names are **1**−**4**, respectively, according to the solvent. Compound **4** is without single-bonded water due to 2-fold coordination of glyme. The topology of the current cobalt dimers is presented via Scheme 1, where L = IPA, 1,4-dioxane, THF, or part of the glyme group. For comparison, the complex $Co_2(\mu\text{-}H_2O)(\mu\text{-}Piv)_2(Piv)_2(HPiv)_4$ (**5**), where Piv is $OOC(CH_3)_3$, has been resynthesized from ref 17 and included in the magnetic and magnetooptical studies.

Scheme 1. Schematic Diagram of Dinuclear Cobalt Compounds Studied in This Work[a]

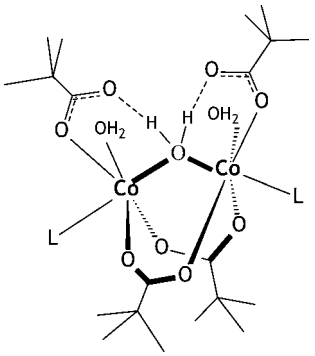

[a]Single-bonded water is present only in **1**−**3**.

As shown in Scheme 1, the central motive has two 6-fold-coordinated Co^{II} ions bridged by the O atom of the water molecule and two substituted carboxylato groups. Depending on the solvent (L) chosen for the preparation, it was possible to obtain four different dicobalt(II) μ-aquo tetrakis-trichloroacetato complexes with slightly different Co···Co and other distances. The distribution of trichloroacetato ligands is retained for each choice of solvent.

By undertaking this work, we wanted to assemble a broad range of experimental data, allowing one to determine the influence of the geometry of the $Co_2(\mu\text{-}H_2O)(\mu\text{-}OOC\text{-}R)_2$ core on the magnetic properties. This includes the search for the influence of coordinating water and coordinating ligands and for the role of hydrogen bridges. We were also interested in the function of coordinating dioxane in **2**, bridged between two dimers and additionally present as an external ligand. Also, the role of solvent molecules in the crystal lattice seemed to be interesting.

The magnetic properties of the dimeric exchange-coupled cobalt complexes depend on the bridges between metal ions. The exchange through water and/or carboxylato bridges is usually weak. However, the magnetic anisotropy of the Co^{II} ion is strong because of the not completely frozen orbital moment in a distorted octahedral position. Unfortunately, the presence of an orbital moment seriously complicates interpretation of the magnetic properties. In this Article, the orbital moment has been explicitly taken into account. In order to obtain unequivocally relevant parameters, we use both temperature- and field-dependent magnetic data and perform simultaneous fits of both of these data sets. Temperature- and field-dependent MCD data sets were used to check the correctness of the interpretation of the magnetic data.

2. EXPERIMENTAL SECTION

2.1. Synthesis. The synthetic strategy to obtain compounds **1**−**4** is generally as follows:

$$CoCO_3(s) \rightarrow Co(CCl_3COO)_2 \cdot nH_2O(s)$$
$$\rightarrow Co_2(\mu\text{-}H_2O)(OOC\text{-}CCl_3)_4(H_2O)_2 \cdot 2L$$

The first step occurs in water and the second step in different solvents (L) with trichloroacetic anhydride (TCA_2O) added to get rid of water.

For instance, the compound $Co_2(\mu\text{-}H_2O)(\mu\text{-}OOC\text{-}CCl_3)_2(OOC\text{-}CCl_3)_2(H_2O)_2(C_4H_8O)_2$ (**3**) was obtained from the reaction of a slurry $CoCO_3$ with a stoichiometric amount of trichloroacetic acid and

dx.doi.org/10.1021/ic202529p | Inorg. Chem. 2012, 51, 6046−6055

Table 1. Crystallographic Data for Complexes 1−4

	1	2	3	4
mol formula	$C_{14}H_{22}Cl_{12}Co_2O_{13}\cdot 2C_3H_8O$	$C_{28}H_{36}Cl_{24}Co_4O_{28}\cdot 4C_4H_8O_2$	$C_{16}H_{22}Cl_{12}Co_2O_{13}\cdot C_2HCl_3O_2$	$C_{16}H_{22}Cl_{12}Co_2O_{13}$
fw	1061.76	2259.50	1128.97	965.60
temperature (K)	100(2)	100(2)	100(2)	100(2)
cryst syst	triclinic	monoclinic	triclinic	orthorhombic
space group	$P\bar{1}$ (No. 2)	$P2_1/c$ (No. 14)	$P\bar{1}$ (No. 2)	*Pbcn* (No. 60)
a (Å)	14.5812(8)	11.657(1)	13.8631(7)	a = 22.5438(6)
b (Å)	15.3195(9)	32.949(3)	14.3824(7)	b = 13.4588(5)
c (Å)	21.850(1)	11.928(1)	23.227(1)	c = 11.6256(5)
α (deg)	94.468(4)	90	80.651(4)	90
β (deg)	96.225(1)	110.174(8)	77.000(4)	90
γ (deg)	116.418(6)	90	62.335(5)	90
volume (Å^3)	4301.5(4)	4300.3(6)	3897.5(3)	3527.4(2)
Z	4	2	4	4
density (calcd) (Mg m^{-3})	1.640	1.745	1.881	1.818
abs coeff (mm^{-1})	1.571	1.583	1.896	1.902
F(000)	2144	2272	2240	1920
cryst size (mm^3)	0.50 × 0.50 × 0.48	0.55 × 0.50 × 0.32	0.50 × 0.40 × 0.40	0.50 × 0.36 × 0.26
θ range for data collection (deg)	2.24−26.37	4.09−26.37	4.09−26.37	2.49−2637
h, *k*, *l* ranges	−17, 18, −19, 19, −26, 27	−14, 14, −41, 39, −14, 14	−16, 17, −17, 17, −28, 28	−28, 28, −16, 16, −14, 14
reflns collected	47463	34970	41338	40135
indep reflns	17457 [*R*(int) = 0.0193]	8693 [*R*(int) = 0.0390]	16117 [*R*(int) = 0.0206]	3611 [*R*(int) = 0.0429]
abs corrn	semiempirical from equivalents	semiempirical from equivalents	semiempirical from equivalents	semiempirical from equivalents
max and min transmn	0.5193 and 0.5071	0.956 and 0.718	0.5176 and 0.4508	0.6276 and 0.4297
data/restrains/param	17457/26/943	8693/143/595	16117/38/944	3611/0/198
GOF on F^2	1.127	1.337	1.018	1.248
final *R* indices [$I > 2\sigma(I)$]	R1 = 0.0362, wR2 = 0.0784	R1 = 0.0871, wR2 = 0.1790	R1 = 0.0602, wR2 = 0.1531	R1 = 0.0337, wR2 = 0.0503
R indices (all data)	R1 = 0.0617, wR2 = 0.0986	R1 = 0.1056, wR2 = 0.1853	R1 = 0.0801, wR2 = 0.1647	R1 = 0.0456, wR2 = 0.0601
largest diff peak and hole (e A^{-3})	1.820 and −1.325	0.659 and −0.673	3.603 and −1.677	0.729 and −0.618

heating to 40 °C until complete dissolution of the solid. After the solution was cooled, long purple needles crystallized. The solid thus formed was redissolved in THF with 0.2 equiv of TCA_2O and filtered warm.

The resulting purple solid was characterized by Fourier transform infrared (FTIR; KBr pellet) spectrometry, which showed the bridging carboxylato stretch as two close bands ($\Delta\nu$: 98 cm^{-1}), while the nonbridging trichloroacetato groups displayed a strong band at 1663 cm^{-1}. The FTIR frequencies are 3226(b), 1663(s), 1352(s), 840(m), 742(m), and 683(m) cm^{-1}.

The preceding reaction in the absence of TCA_2O (as well as the reaction without pivalic anhydride) yielded cobalt(II) monomers $[Co(CCl_3COO)_2\cdot nH_2O]$.

Other compounds were prepared in a similar way, but instead of THF, IPA was used for **1**, 1,4-dioxane in the case of **2**, or glyme in the case of **4**. Compound **5** was resynthesized following the procedure given by Aromi et al.,[17] where the CCl_3 group was replaced by the $C(CH_3)_3$ group.

2.2. XRD. Crystal data were collected using an Oxford Diffraction Xcalibur (TM) single-crystal X-ray diffractometer with a sapphire charge-coupled detector. A full sphere of reciprocal space was scanned by $\varphi-\omega$ scans. Empirical absorption correction using spherical harmonics, implemented in the *SCALE3 ABSPACK* scaling algorithm, was performed by the program *CrysAlisRED*.[18] The structures were solved by direct methods using *SHELXS-97*[19] and refined by full-matrix least squares on F^2 for all data using *SHELXL-97*.[20] H atoms attached to the water O atom were located in the difference Fourier map and allowed to refine freely. All other H atoms were added at calculated positions and refined using a riding model. Isotropic temperature factors of all H atoms were fixed to 1.2 times the equivalent isotropic displacement parameters of the parent atom. Anisotropic thermal displacement parameters were used for all non-H atoms.

2.3. Magnetic and MCD Measurements (Experimental Conditions). Direct-current (dc) magnetization measurements for polycrystalline samples were done with a Quantum Design SQUID magnetometer, model MPMS 5XL. The samples were pressed into pellets in order to avoid reorientation of grains in the magnetic field. All temperature dependencies were measured in a magnetic field of 1000 Oe. Magnetization curves $M(H)$ were measured up to H = 50 or 85 kOe at a constant temperature of 2 or 4 K. The data were corrected for diamagnetism of the sample container and for the core diamagnetic contribution.

VTVH-MCD spectra were measured using a JASCO J-810 spectropolarimeter, interfaced with an Oxford Instruments cryostat Spectromag SM 4000-9T equipped with a split-coil superconducting magnet. The orientation of the field was conventional, i.e., such that the N → S vector pointed toward a photodetector. The samples, thoroughly milled, were mixed with Nujol and placed between two thin plates of fused silica in a copper sample holder that was screwed to the lower end of the sample probe. The temperature was regulated by adjusting the helium gas flow rate from the main bath through the heat exchanger and by using two pairs of heaters and thermometers mounted at the heat exchanger and at the sample probe near the sample. The accuracy of the temperature control was better than 0.1 K. The cryostat windows and the sample holder were checked in order to be sure that they did not contribute to the MCD signals. Data acquisition was achieved using JASCO spectra manager software. The obtained MCD spectra were corrected by subtracting the small zero-field MCD signal.

3. CRYSTAL STRUCTURES AND STRUCTURAL CONSIDERATIONS

The crystal data collection for the four new compounds $C_{14}H_{22}Cl_{12}Co_2O_{13}\cdot 2C_3H_8O$, $C_{28}H_{36}Cl_{24}Co_4O_{28}\cdot 4C_4H_8O_2$, $C_{16}H_{22}Cl_{12}Co_2O_{13}\cdot C_2HCl_3O_2$, $C_{16}H_{22}Cl_{12}Co_2O_{13}$ (abbreviated

dx.doi.org/10.1021/ic202529p | Inorg. Chem. 2012, 51, 6046−6055

as **1**−**4**) is given in Table 1. Corresponding molecular structures are shown in Figures 1−4. All detailed data are

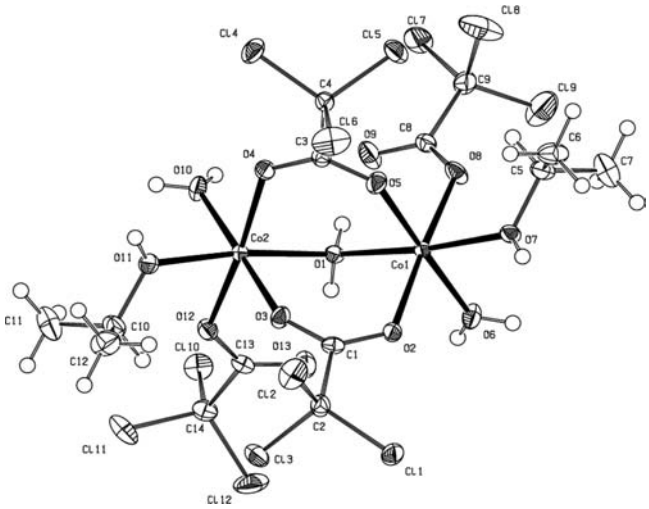

Figure 1. ORTEP diagram of compound **1** at 30% probability. Only one of two crystallographically inequivalent dimers is shown. The two solvent molecules C_4H_8O are omitted for better clarity.

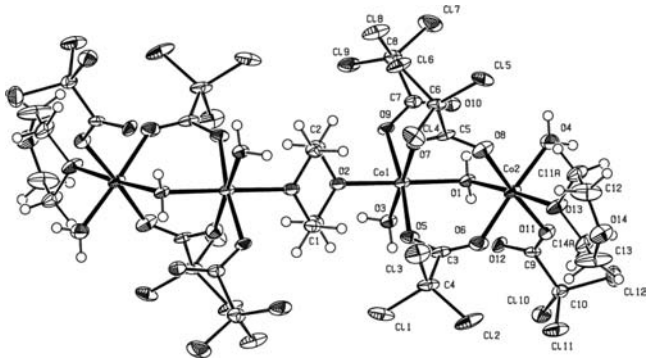

Figure 2. ORTEP diagram of compound **2**. The four solvent molecules $C_4H_8O_2$ are omitted for better clarity.

included in the Supporting Information. Crystal structure data of the fifth compound, $[Co_2(\mu\text{-}OH_2)(\mu\text{-}Piv)_2(Piv)_2\ (HPiv)_4]$ (molecular formula $C_{40}H_{78}Co_2O_{17}$), can be found in ref 17. The space group of **5** is $P2_1/n$.

Compounds **1**−**3** have solvent molecules in their crystal lattices: IPA, 1,4-dioxane, and trichloroacetic acid, respectively. In **2**, some atoms of the crystal solvent are disordered. The same applies to the atoms C11 and C14 attached to O (of the external 1,4-dioxane ring) bonded to Co. As a result of this, the refinement for **2** stopped at R1 = 0.0871.

All compounds except of **2** are dimeric. The packing of molecules in the crystal structures of **1** and **3** is similar. Both compounds crystallize in the space group $P\bar{1}$ with two kinds of dimers, which are crystallographically different but differ only slightly. Compound **2**, formally tetrameric, is composed of two crystallographically equivalent dimeric complexes linked via 1,4-dioxane, the midpoint of which occupies a center of symmetry (see Figure 2). The dimeric molecule **4**, most symmetrical of all of the studied compounds, has a 2-fold symmetry axis due to occupation of the O atom of the bridging water at the special 4c position of the space group *Pbcn*. Cobalt in all five complexes **1**−**5** is quasi-octahedrally bonded to six O atoms. The Co···O

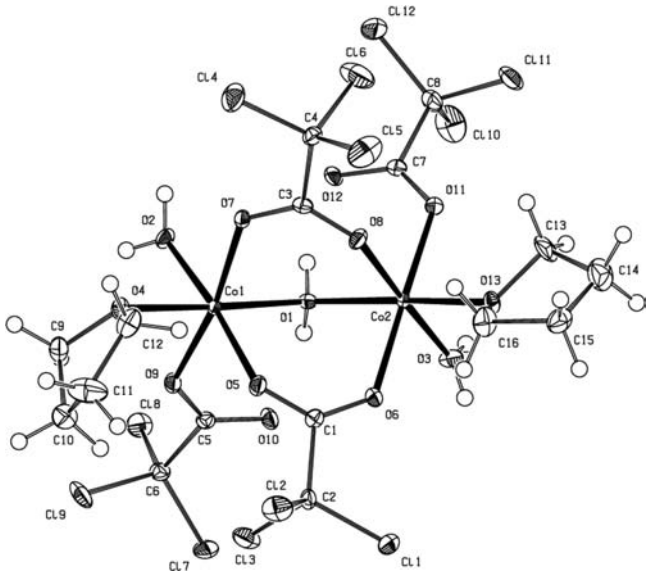

Figure 3. ORTEP diagram of compound **3**. Only one of two crystallographically inequivalent dimers is shown. The solvent molecule $C_2HCl_3O_2$ is omitted for better clarity.

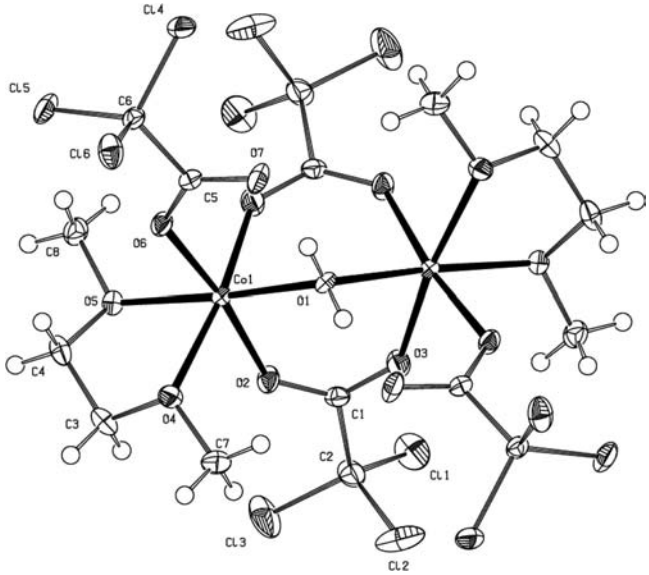

Figure 4. ORTEP diagram of compound **4**.

distances are shown in Table 2. The detailed coordination around one Co ion in each of the complexes is as follows: for **1**, there are two O atoms from OH_2 groups, one is bridging and one is single-bonded, three O atoms from the $OOC-CCl_3$ groups, and one terminal O atom from IPA, $OHCH(CH_3)_2$; for **2**, it is the same as that for **1** except the terminal O atom is from dioxane, $C_4H_8O_2$; one Co bonds one external dioxane and the second Co bonds to an O atom from the bridging dioxane group; for **3**, the same as for **1**, but the terminal group is oxygen from THF, $(CH_2)_4O$; for **4**, it is the same as that for **1** except there is no single-bonded water because two O atoms from the glyme group occupy the external positions; for **5**, there is one O atom from the bridging water, two O atoms from the bridging trimethyloacetato groups, two O atoms from two protonated pivalates and one O atom from one deprotonated pivalate. As in **4**, there is no single-bonded water. Hence, each Co of each

dx.doi.org/10.1021/ic202529p | *Inorg. Chem.* 2012, 51, 6046−6055

Table 2. Co−O Distances for Complexes 1−4[a]

	1						3				
	dimer 1		dimer 2		2		dimer 1		dimer 2		4
	n = 1	n = 2	n = 3	n = 4	n = 1	n = 2	n = 1	n = 2	n = 3	n = 4	n = 1
Con−O_{br}	2.136(2)	2.138(2)	2.149(2)	2.162(2)	2.124(5)	2.142(5)	2.120(3)	2.122(3)	2.133(3)	2.120(3)	2.1479(12)
Con−O	2.074(2)	2.063(2)	2.057(2)	2.038(2)	2.057(5)	2.039(5)	2.104(3)	2.020(3)	2.094(3)	2.029(3)	2.1494(16)
Con−O_{term}	2.074(2)	2.073(2)	2.080(2)	2.096(2)	2.098(5)	2.150(5)	2.155(3)	2.092(3)	2.160(3)	2.078(3)	2.1220(16)
Con−O_{Ac1br}	2.126(2)	2.033(2)	2.134(2)	2.019(2)	2.062(5)	2.059(6)	2.090(3)	2.052(3)	2.080(3)	2.045(3)	2.0322(17)
Con−O_{Ac2br}	2.046(2)	2.106(2)	2.033(2)	2.121(2)	2.068(5)	2.061(6)	2.047(3)	2.079(3)	2.060(3)	2.068(3)	2.0322(17)
Con−O_{Ac}	2.111(2)	2.121(2)	2.112(2)	2.125(2)	2.082(5)	2.060(6)	2.064(3)	2.131(3)	2.068(3)	2.118(3)	2.0651(17)

[a] O_{br} = H_2O bridge; O = single-bonded water, for **4** O_{glym}; O_{term} = for **1** IPA, for **2** dioxane, for **3** THF, for **4** O_{glym}; O_{Ac1br} = one acetate bridge; O_{Ac2br} = second acetate bridge; O_{Ac} = acetate.

Table 3. Co···Co Distances, Co−O_{br}−Co Angles, and Dihedral Angles

	1			3			
	dimer 1	dimer 2	2	dimer 1	dimer 2	4	5[a]
Co···Co distances (Å)	3.642(3)	3.665(3)	3.610(5)	3.597(3)	3.606(3)	3.594(2)	3.430(2)
Co−O_{br}−Co angle (deg)	117.18(10)	116.45(10)	115.6(2)	116.00(15)	115.96(14)	113.59(10)	111.38(10)
dihedral O_{aqua}−Con··· Co(n+1)−O_{aqua} angles (deg)	92.93	92.09	102.67	82.51	82.09		
dihedral O_{Ac}−Con··· Co(n+1)−O_{Ac} angles (deg)[b]	83.99	82.07	86.76	92.49	96.84	89.06	72.71

[a] This work. [b] For **5**, the dihedral angle reads for O_{piv}−Co(1)···Co(1′)−O_{piv}′.

Table 4. Distances for Hydrogen Bridges O_{br}−H···O_{Ac} for 1−4 or O_{br}−H···O_{Piv} for 5 and Related Angles

	units	dimer 1		dimer 2		average
1	Å	2.563(3)	2.567(3)	2.580(3)	2.583(3)	2.573(3)
	deg	165.58	165.22	170.65	164.19	166.41
2	Å	2.615(7)	2.583(7)			2.599(7)
	deg	148.49	166.36			157.43
3	Å	2.594(5)	2.618(5)	2.618(5)	2.618(5)	2.612(5)
	deg	163.22	151.00	160.29	149.13	155.91
4	Å	2.561(2)				2.561(2)
	deg	171.92				171.92
5[a]	Å	2.541(3)	2.531(2)			2.536(2)
	deg	164.81	165.81			165.31

[a] Calculated based on our structural data.

dimeric unit is triply bridged by one O atom from water and two O atoms from trichloracetato or pivalato groups.

The longest Co−O_{br} distance, with 2.162(2) Å, is realized in one of the dimers of **1**, while the shortest one with 2.120(3) Å belongs to both dimers of **3**. The Co−O distance to the single-bonded water is between 2.020(3) and 2.094(3) Å. In **4**, the O atom from glyme occupies the water positions of **1**−**3** with a Co−O distance equal to 2.1494(16) Å. For **1**, the Co−O distances to the bridged trichloroacetate groups are slightly different [longest 2.134(2) Å; shortest 2.019(2) Å] and the same for **3** [longest 2.090(3) A; shortest 2.045(3) Å]; for **2** and **4**, they are equal within the error limit [2.063(6) Å and 2.0322(17) Å, respectively]. All bond angles of coordinated groups around each Co are in the normal range (see CIF files in the Supporting Information).

Table 3 shows the Con−O_{br}−Co(n+1) angles ranging from 117.18(10)° for one dimer of **1** to 113.59(10)° for **4**. The comparable angle for **5**, 111.38(6)°, is still lower. As for dihedral angles, the most outstanding value is for O_{aqua}−Con···Co(n+1)−O_{aqua} angle of **2**, which equals to 102.6°, while the lowest value is for **3**, being 82°. The Co1···Co2 distances for **2**−**4** do not differ much themselves, being on the average 3.602 Å; for **1**, this distance is considerably greater, 3.665 Å, but for **5**, it is lower and equals to 3.430 Å. This can be explained as being due to the steric effects of the CCl_3 group compared to the $C(CH_3)_3$ group in **5**. These Co1···Co2 distances in Table 3 are similar to those found in protein structures; however, we should note that not all protein data[21] were obtained at a resolution comparable to that of these model compounds.

The existing hydrogen bonds (Table 4), characteristic for all complexes, are between the bridging O atom O_{br} and the terminal monodentate carboxylato/pivalato groups; see Scheme 1. Basically, all of these hydrogen bridges increase the stiffness of the complex core. This leads to a very comparable $Co_2(\mu$-$H_2O)(\mu$-OOC-R)$_2$ core structure, even evidenced by the angle on hydrogen (Table 4). In fact, the dipoles O−H and H···O have a very similar orientation. Additionally, in **5**, one O atom of the pivalato ion is bonded to the terminal pivalato group via hydrogen bridges; see ref 17.

In all cases, the distance of O_{br}−H is in the limits of 0.80−0.90 Å and is about 2 times lower than the H···O distance, confirming that the bridging O atom belongs to water. This has some influence on the magnetic properties because the exchange coupling via the O atom is different from that via the water group; see section 5.

dx.doi.org/10.1021/ic202529p | Inorg. Chem. 2012, 51, 6046−6055

The O_{br}—H···O bond has the shortest length for **5** equal to 2.536(2) Å; for **4**, this length is 2.561(2) Å, for **1** 2.573 (3) Å, for **2** 2.599(5) Å, and for **3** 2.612(5) Å, all on average. The small increase of the length of the hydrogen bridges of **1**—**4** compared to **5** can be considered to be due to the space-filling CCl_3 groups. The hydrogen bridges presented in Table 4 are nonsymmetric (see the Supporting Information); the average angle is 163.40°, the largest 171.92°, and the smallest 148.49°.

4. MAGNETIC AND VTVH-MCD DATA AND THEIR ANALYSIS

4.1. Magnetic Susceptibility Analysis. The magnetic properties of the investigated complexes are presented in Figure 5 and in the Supporting Information. The χT (χ = magnetic susceptibility) behavior for all compounds looks similar and indicates an antiferromagnetic coupling between Co ions. However, the low-temperature values of the χT product demonstrate that the absolute values of the exchange parameter are different in spite of the similar bridging part for all complexes. The room temperature χT values range from 6.1 emu K mol^{-1} for **3** and **4** to 6.92 emu K mol^{-1} for **1**. Because typical values of the exchange parameters in the exchange-coupled cobalt(II) complexes are about several wavenumbers,[22] these differences in the magnetic behavior at room temperature might be mainly due to the local anisotropy (low-symmetry crystal-field term) of the Co ions.

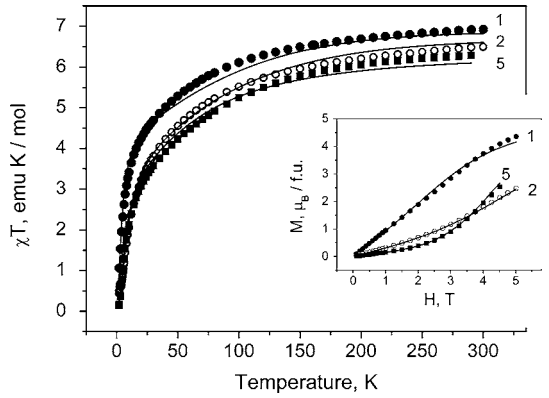

Figure 5. Experimental magnetic susceptibility multiplied by the temperature for **1**, **2**, and **5** shown as a function of the temperature. Inset: magnetization versus magnetic field measured at 2 K (complexes **1** and **5**) and 4 K (complex **2**). Theoretical curves (solid lines) are calculated at parameters presented in Table 5. See also the Supporting Information for the data of complexes **3** and **4**.

The magnetization versus magnetic field behavior is shown in the inset of Figure 5 (see also the Supporting Information). For complex **2**, there exists some singularity in the $\chi(T)$ curve at temperature 2.9 K as detected by dc and alternating-current magnetic measurements. We interpret this as a ferromagnetic transition occurring in an impurity (the bulk ferromagnetic transition is not possible in this structure). This small contamination (certainly below 1%) does not influence the magnetic properties above 4.0 K. Because the present study is focused on the investigations of the behavior of the exchange-coupled cobalt dimers, for this complex, the magnetization data at 4 K were analyzed. It was assumed that at this and higher temperatures the interdimer interaction can be neglected and the compound behaves as a paramagnetic collection of the isolated cobalt dimers. For the other four complexes, the magnetization data were collected at 2 K. The magnetization versus magnetic field behavior of investigated complexes differs remarkably from each other in both field dependences and absolute values. For complexes **1** and **4**, $M(H)$ represents almost straight lines with values of 4.36 and 3.8 μ_B at H = 5 T, respectively, while for complexes **2**, **3**, and **5**, the corresponding curves are concave [for complex **3**, the magnetization measurements were performed up to 8.5 T, and at magnetic fields higher than 5 T, $M(H)$ starts to saturate].

The model for theoretical analysis of the experimental behavior of the exchange-coupled high-spin cobalt(II) dimers is presented in detail in the review article.[23] Here, for a definition of the parameters, we evoke only the Hamiltonian. It consists of the spin—orbit coupling, low-symmetry (noncubic) crystal-field term, magnetic exchange between Co ions, and Zeeman interaction:

$$\boldsymbol{H} = \sum_{i=1,2}\left(-\frac{3}{2}\kappa_i\lambda\boldsymbol{S}_i\boldsymbol{L}_i + \boldsymbol{L}_i\boldsymbol{\Delta}_i\boldsymbol{L}_i + \mu_B\left[g_0\boldsymbol{S}_i - \frac{3}{2}\kappa_i\boldsymbol{L}_i\right]H\right) - 2J_{ex}\boldsymbol{S}_1\boldsymbol{S}_2 \quad (1)$$

In eq 1, κ is the orbital reduction factor and $\lambda = -170$ cm^{-1} is the spin—orbit coupling parameter for a free Co^{II} ion. Zeeman interaction for high-spin Co^{II} consists of both spin and orbital contributions. Magnetic exchange between two Co ions is assumed to be isotropic and operates between real spins.[24] For more details, see ref 23 and the Supporting Information.

The magnetic properties of interacting Co^{II} ions (especially at low temperatures) strongly depend on the relative orientation of the principal axes of the local $\boldsymbol{\Delta}$ tensors. The distortion from the octahedral surroundings is assumed to be axial, with Δ_i being the axial parameter of the $\boldsymbol{\Delta}_i$ tensor. Both the directions of the local coordinate axes and the type of distortion (elongation or compression) were found by diagonalization of the crystal-field gradient tensor.[25] The O atom of the water molecule differs significantly from the O atoms of other ligands. To account for this difference, the whole molecule of water was used in the calculation of the crystal-field gradient tensor; namely, along with the negative charge of the water O atom, two positive point charges were set at the positions of the water H atoms.

Because calculation of the crystal-field gradient tensor is based on some approximations, we allow the angle α between the local coordinate axes of the Co ions to deviate slightly from the values obtained in this procedure. To reduce the number of parameters, we assumed $\kappa_1 = \kappa_2$. Best-fit parameters for all complexes are listed in Table 5. The corresponding theoretical curves are presented in Figure 5 as solid lines.

One can see that the values of the exchange parameters for all complexes are small. This weak exchange interaction is caused by the fact that the three bridging groups do not provide a good pathway for the exchange interaction. The values of the orbital reduction factor lie between the weak field limit (κ = 1)

Table 5. Best-Fit Parameters for Compounds 1—5

complex	α, deg	Δ_1, cm^{-1}	Δ_2, cm^{-1}	κ	J_{ex}, cm^{-1}
1	110	−1300	−870	1	−1.5
2	110	−1200	480	0.97	−2.1
3	130	−1300	880	0.85	−2.1
4	115	−1000	−1000	0.81	−1.5
5	130	560	660	0.86	−1.6

dx.doi.org/10.1021/ic202529p | Inorg. Chem. 2012, 51, 6046—6055

and the average value (κ = 0.8). We turn our attention to the pronounced differentiation of the Δ parameters.

The values of the Δ_i parameters indicate that for **1** and **4** the distortion of the local surroundings can be described as an axial compression for both Co ions, for **5** both local surroundings are axially elongated, while for **2** and **3** the octahedron around one Co ion is axially compressed and that around another one is axially elongated.

For all complexes excluding **4**, these observations are in good agreement with the analysis based on the crystal-field gradient tensor study. As for complex **4**, theoretical analysis, based on the crystal-field gradient tensor, predicts inequality, $\Delta_1 = \Delta_2 > 0$ (equality, $\Delta_1 = \Delta_2$, results from symmetry). All attempts to describe the experimental data with positive Δ_i parameters failed. The possible reason for this disagreement can be due to the fact that the crystal-field gradient tensor is calculated by taking into account point charges of the nearest ligands and neglecting all other types of interactions. Accounting for other interactions between the metal ion and the ligands can lead to a change of the relative energies of the d_{xy} and $d_{xz}(d_{yz})$ orbitals. In turn, it leads to a change of the sign of the corresponding Δ_i parameters.

It should be mentioned that the low-temperature magnetization behavior of the exchange-coupled cobalt dimers is determined not only by the strength of the exchange interaction but also by the magnitude and type of low-symmetry distortions around each interacting ion. As a result, complexes with the same values of J_{ex} can demonstrate different $M(H)$ behavior (compare **1** and **5**) and vice versa, that is, similar $M(H)$ curves can be demonstrated by dimers with different values of the exchange parameter (for example, complexes **2** and **5**).

4.2. MCD Spectroscopy Data Analysis. MCD spectra of all investigated compounds show a broad band at about 500 nm (Figure 6 and the Supporting Information). For complexes **1**, **4**, and **5**, this band is located at 505 nm, while for **2** and **3**, it is shifted to 490 and 510 nm, respectively. The energy of this MCD band is characteristic for d−d transitions, namely, for transitions to the $^4T_{1g}$ state.[26,27] In the low-symmetry field, the excited $^4T_{1g}$ term is split, and it results in the shoulders in MCD spectra for complexes **1**, **2**, and **5**. In **3** and **4**, these shoulders are not seen, most probably because of the broad strong main band. A similar MCD spectrum was reported for $[Co_2(\mu\text{-}OAc)_3(urea)(tmen)_2][OTf]$; see ref 28, where the magneto-optical investigation of this ferromagnetically coupled cobalt dimer was presented.

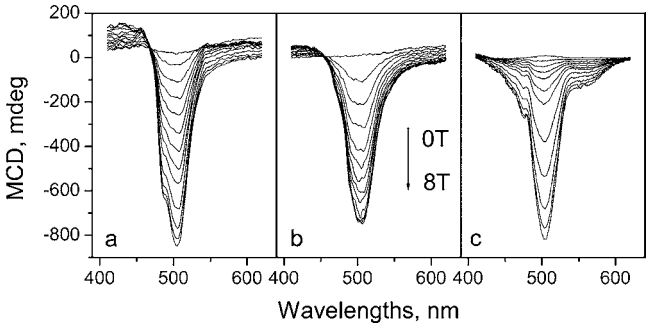

Figure 6. Experimental MCD spectra of **1** in panel a, **4** in panel b, and **5** in panel c obtained at 3 K and different values of the magnetic field.

The magnetization saturation behavior of all five complexes can be analyzed with use of the following equation:[29]

$$\Delta\varepsilon \propto \sum_{n=1,2} M_{xy}(n)\,\langle \bar{L}_z(n)\rangle_T + M_{yz}(n)\,\langle \bar{L}_x(n)\rangle_T + M_{zx}(n)\,\langle \bar{L}_y(n)\rangle_T \quad (2)$$

where $\langle \bar{L}_k(n)\rangle_T$ is the thermally and orientationally averaged kth component of the orbital angular momentum of the nth Co ion within the ground state of the whole dimer. $M_{ij}(n)$ parameters represent combinations of the matrix elements of the ith and jth components of the electric dipole operator and are equal to those for a noninteracting nth Co ion. See all details in the Supporting Information.

In general, for the case of the nonsymmetric dimeric complex, there are six $M_{ij}(n)$ parameters, and the problem is overparametrized. However, the number of these parameters can be reduced. Figure 7 shows the $\langle \bar{L}_k(n)\rangle_T$ values calculated at T = 3 K and H = 8 T as a function of the axial distortion assuming the absence of the exchange interaction within the dimer. One can see that, for the case when the local octahedron is axially compressed, the $\langle \bar{L}_k\rangle_T$ component parallel to the compression axis significantly exceeds the perpendicular components. In the limit of strong compression, the components of the orbital angular momentum perpendicular to the compression axis are completely quenched. In this limiting case, the main contribution to the MCD spectrum comes from the xy-polarized optical transitions. Transitions of other polarizations appear in the MCD spectrum as a result of the spin−orbit admixture of some states to the ground and/or excited states,[30,5b] and the corresponding contributions are weak. The axial elongation results in the opposite effect: the perpendicular components of **L** exceed the parallel one. So, one can conclude that for this type of distortion the contributions of the xz- and yz-polarized transitions dominate in the MCD spectrum. The account of the exchange interaction changes the behavior of the $\langle \bar{L}_k\rangle_T$ components presented in Figure 7. However, the conclusion remains the same: the contributions from ions in the axially compressed surroundings are mainly xy-polarized, while for axial elongation, the corresponding transitions are xz- and yz-polarized. In addition, because in this consideration, we restrict ourselves to axial distortion of the octahedral surroundings, we set $M_{xz}(n) = M_{yz}(n)$ and the number of $M_{ij}(n)$ parameters in eq 2 is reduced from six to two.

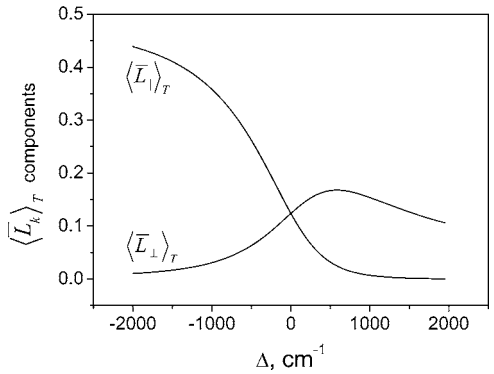

Figure 7. Dependence of the $\langle \bar{L}_k\rangle_T$ components on the parameter Δ calculated at 3 K and 8 T.

To construct the saturation magnetization curves, we recorded signal intensities at the maximum of the strong

dx.doi.org/10.1021/ic202529p | Inorg. Chem. 2012, 51, 6046−6055

main band. The results are shown in Figure 8 and in the Supporting Information. The obtained MCD saturation

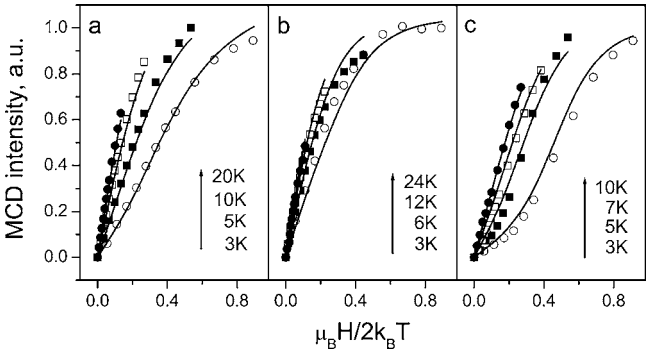

Figure 8. Magnetization curves at 505 nm: (a) for complex **1**, theoretical curves are calculated at the assumptions $M_{ij}(1) = M_{ij}(2)$ and $M_{xz}(n) = M_{yz}(n) = 5.5M_{xy}(n)$; (b) for complex **4**, theoretical curves are calculated at the assumption $M_{xy}(1) = M_{xy}(2)$ [other $M_{ij}(n)$ parameters are negligible]; (c) for complex **5**, theoretical curves are calculated at the assumption $M_{xz}(1) = M_{yz}(1) = M_{xz}(2) = M_{yz}(2)$ [other $M_{ij}(n)$ parameters are negligible].

magnetization curves demonstrate different types of behavior. For complex **5**, at small values of the magnetic field, there is a slower growth of the signal intensity. With an increase of the magnetic field magnitude, the growth rate of the signal increases. For complex **4**, on the contrary, there is a sharp increase in the signal intensity already at small values of the magnetic field. With the growth of the magnetic field, the signal intensity saturates. The saturation magnetization curves for complexes **1**−**3** demonstrate behavior intermediate between these two cases.

The temperature and magnetic field behavior of the MCD signal of all five complexes were modeled using the best-fit parameters obtained at the previous stage of investigation during analysis of the magnetic data. The results are shown in Figure 8 as solid lines (see also the Supporting Information). For complexes **2**−**5**, the MCD saturation behavior is well reproduced at the above assumption that contributions from ions in the axially compressed surroundings are *xy*-polarized, while for the axial elongation, the corresponding transitions are *xz*- and *yz*-polarized. The ratios between nonzero $M_{ij}(n)$ parameters are given in the figure captions. As for complex **1**, all attempts to reproduce the MCD behavior using only the *xy*-polarized contribution fail. The agreement with the experiment can be obtained only at the assumption that transitions of all polarizations contribute to the MCD signal. This can be caused by the fact that the value of the axial Δ parameter for ion 2 ($\Delta_2 = -870$ cm^{-1}) is not strong enough to quench completely the components of the orbital angular momentum perpendicular to the compression axis (see Figure 7). As a result, a contribution of all polarizations to the entire MCD signal is significant. It should be noted that the theoretical curves presented in Figure 8 are not a result of the best-fit procedure and only demonstrate that the saturation behavior of the MCD signal can be well reproduced using the parameters obtained during the fit of the magnetic data and our assumptions about polarization of the corresponding optical transitions. It should be mentioned once again that polarization of the MCD transitions corresponds to the local coordinate system of the corresponding Co ion.

5. DISCUSSION

In the present contribution, the magnetooptical investigation of the family of cobalt(II) dimers with the same central part and different terminal ligands is described. It was shown that the resultant exchange through water and two carboxylato groups is weakly antiferromagnetic.

No influence of the solvent molecules in the crystal structures of **1**−**3** on the magnetic coupling is observed. A change of the terminal ligands has a small effect on the magnitude of the exchange interactions, mainly because of the small change of the distances between Co ions and the bridging O atom of water and/or carboxylato groups. In contrast, a change of the terminal ligands strongly affects both the value of the low-symmetry fields and the direction of the local anisotropy axes. Because the Co^{II} ion possesses the unquenched orbital angular momentum, its magnetic properties (and, as a consequence, the magnetic behavior of the whole dimer) strongly depend on the value and the sign of this low-symmetry field.

It should be noted that Kanamori−Goodenogh rules[31] do not predict the sign of the 90° interaction for Co^{II} ions. Instead, the 180° interaction is predicted to be antiferromagnetic. Thus, there is a possibility that the weakness of interactions in **1**−**5** is caused by the partial cancellation of coupling. If this is accidental, a significant change of coupling would be observed in slightly modified systems. However, this does not take place, as confirmed through a review of the literature (see below). Thus, the coupling through the O atom of water is certainly antiferromagnetic in **1**−**5**.

A number of dimeric/oligomeric high-spin cobalt(II) compounds with bonding schemes similar to those in **1**−**5** were reported, and their magnetic properties were described. A comparison of the literature and our data may be interesting. However, in some of the papers, authors concentrate on the magnetic coupling only, not paying attention to the orbital moment and crystal-field parameters. This can be substantiated by taking into account the fact that, in the case of a strong axial elongation of the local surroundings (big positive Δ parameter), the orbital angular momentum disappears and the octahedrally coordinated Co^{II} ion can be regarded as a spin-only system with $S = {}^3/_2$.[23,32] The influence of the orbital momentum is incorporated into the principal values of both the local zero-field-splitting tensor and the local **g** tensor. An example of such an approach may be the paper of Schultz et al.[33] They studied binuclear complexes of the formula $M_2(\mu\text{-}H_2O)(\mu\text{-}OAc)_2(OAc)_2(Im)_4$, where M= Mn, Co, or Ni, designed as mimics of the active sites of hydrolase enzymes. These complexes have a μ-aquo bis(μ-carboxylato) dimeric core, with four terminal imidazole ligands and two terminal carboxylate ligands within the molecule. The terminal carboxylates form a hydrogen-bond with the bridging aqua ligand, similarly to complexes **1**−**5**. For M = Co, the antiferromagnetic coupling was observed with a J_{ex} value equal to −1.60 cm^{-1}. The value of the relevant $Co-O_{br}-Co$ bridging angle 117.2° is the same as that for one dimer of our complex **1** (see Table 3); the reported Co···Co distance is 3.687 Å. As seen (Table 5), also the values of J_{ex} are nearly equal to each other.

The next example from this series that we would like to quote is a novel chain compound $[[Co_2(\mu\text{-}OH_2)(\mu\text{-}Piv)_2(Piv)_2](\mu\text{-}bpym)]_n$,[34] consisting of alternating bipyrimidine bridges linking the dimeric units $[Co_2(\mu\text{-}OH_2)(\mu\text{-}$

dx.doi.org/10.1021/ic202529p | Inorg. Chem. 2012, 51, 6046−6055

$Piv)_2(Piv)_2]$. Its water bridge has a reduced value of the bridging angle 108.7°. Similarly to **5**, there exist also two carboxylate bridges; however, two terminal cobalt nearest neighbors are not O but N atoms of the bipyrimidine. The Co···Co intradimer distance is 3.515 Å, longer than 3.430 Å in **5**, and the closest interdimer Co···Co distance is 5.587 Å. The overall coupling is antiferromagnetic with the J_{ex} value ∼−3 cm^{-1} (obtained by the assumption of no orbital moment). This value is about 2 times greater than that obtained for **5**.

Now, several examples of the second group of papers will be given, where the magnetic coupling was analyzed by the assumption of the presence of spin−orbit interaction and a distortion of the coordination octahedron. The first example is already mentioned in the Introduction section: the trimeric chain compound[16] $[Co_3(\mu\text{-}H_2O)_2(\mu\text{-}OOC\text{-}R)_4(OOC\text{-}R)_2(H_2O)_2(C_4H_8O_2)]\cdot 2C_4H_8O_2$ with R = CF_3, having the same bridging motive as **1**−**5**. The value of the Co−O_{aqua}−Co angle here is 115.1°, thus nearly the same as that for our **2**, but the value of the magnetic coupling is very small, J_{ex} = −0.4 cm^{-1}. The values of the crystal-field-splitting parameters are Δ_1 = −970 cm^{-1} and $\Delta_2 = \Delta_3$ = +1160 cm^{-1}.

The next example refers also to R = CF_3, but the water bridging O atom is replaced by another kind of bridging O atom. Two cobalt trimers $[Co_3(\mu\text{-}OCC\text{-}R)_4(\mu\text{-}BA)_2(tmen)_2]$ and $[Co_3(\mu\text{-}OCC\text{-}R)_4(\mu\text{-}AA)_2(tmen)_2]$, with Co in distorted octahedral coordination, and each Co pair triply bridged by two trifluoroacetates and one O atom of the benzohydroxamate (BA) or acetohydroxamate (AA) group, respectively, has Co−O_{BA}−Co and Co−O_{AA}−Co angles of 118.5° and 119.3°, respectively.[25] These values are comparable, but the J_{ex} values are remarkably different. They are equal to −3 and −6 cm^{-1}, respectively. Their differentiation points to the influence of the group to which the bridging O atom belongs. The values of the crystal-field parameters are Δ_1 = +372 cm^{-1} and $\Delta_2 = \Delta_3$ = −775 cm^{-1} for the BA compound and Δ_1 = +645 cm^{1} and $\Delta_2 = \Delta_3$ = −642 cm^{-1} for the AA compound. Thus, they are not differentiated much.

It is well-known that, for the series OH_2, OH, and O, the degree of protonation of the bridging O atom strongly influences the magnetic coupling, so that $|J_{ex,H_2O}| < |J_{ex,OH}| < |J_{ex,O}|$. In particular, for some groups to which the bridging O atom belongs, ferromagnetic coupling is possible. There were reports of ferromagnetic coupling in cobalt complexes with carboxylate plus oxo, hydroxo, or even aqua bridges; however, the last case is doubtful (see below).

In the $[Co_2(\mu\text{-}OAc)_3(urea)(tmen)_2][OTf]$ compound[28] (urease model complex), the Co atoms are coupled by two carboxylates and one $O_{carboxylate}$ bridges with the Co−O_{br}−Co angle equal to 107.7°. There is no aqua bridge. The Co−O distance is 2.16 Å (average value), and the Co1···Co2 distance is 3.48 Å. The value of the exchange parameter is J_{ex} = +18 cm^{-1}. The Δ value obtained is equal to +180 cm^{-1}.

Fabelo et al.[14] studied the influence of the bridge on the magnetic coupling in two dicobalt complexes, $[Co_2(bta)(H_2O)_6]_n\cdot 2nH_2O$ and $[Co(phda)(H_2O)]_n\cdot nH_2O$ (H_4bta = 1,2,4,5-benzenetetracarboxylic acid; H_2phda = 1,4-phenylenediacetic acid), with distorted octahedral cobalt coordination. For each compound, the complexes are formed into chains; however, the distances between dicobalt units are large. Co atoms in dimers are triply coupled by μ-aqua, μ-COO(syn−syn carboxylate), and μ-oxo(carboxylate) bridges. The resulting coupling is ferromagnetic. According to the authors, the ferromagnetic coupling originated from μ-aqua and μ-$O_{carboxylate}$ mediation because of the reduced values of the bonding angles Co−O_{aqua}−Co and Co−$O_{carboxylate}$−Co, which are equal to 94° and 92° for $[Co_2(bta)(H_2O)_6]_n\cdot 2nH_2O$ and 93° and 99° for $[Co(phda)(H_2O)]_n\cdot nH_2O$, respectively. The obtained values of the J_{ex} exchange parameter were +2.7 by Δ = −900 cm^{-1} and +1.08 cm^{-1} by Δ = +480 cm^{-1} for $[Co_2(bta)(H_2O)_6]_n\cdot 2nH_2O$ and $[Co(phda)(H_2O)]_n\cdot nH_2O$, respectively. These lower values of J_{ex} in comparison with the previous example (+18 cm^{-1}) may result just from the presence of an aqua bridge, usually bringing negative coupling.

In the above discussion, the richness of the factors responsible for variation of the magnetic coupling in the relative cobalt complexes of the $Co_2(\mu\text{-}O_{br})(\mu\text{-}OOC\text{-}R)_2L$ series was shown. In order of priority, they are the kind of group to which O_{br} belongs, the Co−O_{br}−Co angle, the kind of R group, and the kind of terminal ligand L. Because the compounds of series **1**−**4** differ only in L, they show a small differentiation of the J_{ex} parameter, but the large distribution of Δ is just due to L. Table 6 provides a short compilation of the examples given in the discussion.

Table 6. Bridge Types with Bridging Angle α and Exchange Parameters for Some Selected Cobalt Complexes[a]

complex	bridge, α, deg	J_{ex}, cm^{-1}	ref
$Co_2(\mu\text{-}H_2O)(\mu\text{-}OAc)_2(OAc)_2(Im)_4$[b]	aqua, 117.2 2× carboxylate	−1.6	33
$[[Co_2(\mu\text{-}H_2O)(\mu\text{-}Piv)_2(Piv)_2](\mu\text{-}bpym)]_n$	aqua, 108.7 2× carboxylate	−3	34
$[Co_3(\mu\text{-}H_2O)_2(\mu\text{-}OOC\text{-}CF_3)_4(OOC\text{-}CF_3)_2(H_2O)_2(C_4H_8O_2)]\cdot 2C_4H_8O_2$	aqua, 115.1 2× carboxylate	−0.4	16
$[Co_3(\mu\text{-}OOC\text{-}CF_3)_4(\mu\text{-}BA)_2(tmen)_2]$[c]	O of BA, 118.5 2× carboxylate	−3.1	25
$[Co_3(\mu\text{-}OOC\text{-}CF_3)_4(\mu\text{-}AA)_2(tmen)_2]$[d]	O of AA, 119.3 2× carboxylate	−6.4	25
$[Co_2(\mu\text{-}OAc)_3(urea)(tmen)_2][OTf]$	O of OAc, 107.7 2× carboxylate	+18.0	28
$[Co_2(bta)(H_2O)_6]_n\cdot 2nH_2O$[e]	aqua, 94 O-carboxylate, 92 carboxylate	+2.7	14
$[Co(phda)(H_2O)]_n\cdot nH_2O$[f]	aqua, 93 O-carboxylate, 99 carboxylate	+1.08	14

[a]All compounds are triply bridged through carboxylate OC(R)O groups and the O ion belonging to water or another group. [b]OAc = acetate. [c]BA = benzohydroxamate. [d]AA = acetohydroxamate. [e]H_4bta = 1,2,4,5-benzenetetracarboxylic acid. [f]H_2phda = 1,4-phenylenediacetic acid.

In this work, we showed the influence of the terminal ligands L. They cause rather subtle differentiation of the magnetic coupling, but they strongly influence the crystal-field splitting, having a significant effect on the magnetic properties of cobalt(II) dimers in the whole temperature range. This point may be worth further study to understand the involvement of the catalytic and (bio)catalytic processes of such kinds of dimeric units that are triply bridged by one water and two carboxylato units.

■ ASSOCIATED CONTENT

Ⓢ Supporting Information

X-ray crystallographic files for **1**−**5** in CIF format, theoretical model for magnetic data analysis, temperature- and field-dependent magnetic data for **3** and **4**, MCD spectra for **2** and **3**,

dx.doi.org/10.1021/ic202529p | Inorg. Chem. 2012, 51, 6046−6055

and MCD magnetization curves for **2** and **3** fitted by the assumption of the determined polarization. This material is available free of charge via the Internet at http://pubs.acs.org.

AUTHOR INFORMATION

Corresponding Author

*E-mail: haase@chemie.tu-darmstadt.de (W.H.), z.tomkowicz@uj.edu.pl (Z.T.).

Notes

The authors declare no competing financial interest.

ACKNOWLEDGMENTS

W.H. thanks the German Science Foundation for support in the scope of the Priority Program HA782/85. W.H. and S.O. thank the German Science Foundation for Project HA 782/100-1 in the scope of the Initiation and Enhancement of Bilateral Cooperation program. Z.T. is grateful for a grant of Ministry of Science and Higher Education, Poland (Grant N N202 103238) and the Polish Innovation Economy Operational Program (Contract POIG.02.01.00-12-023/08). We are thankful to Professor Bezborodov for outlining some synthetic routes to obtain compounds **1** and **4**. V.C.-P. acknowledges support of the Department of Inorganic and Analytical Chemistry, Facultad Ciencias Químicas y Farmacéuticas, Universidad de Chile.

REFERENCES

(1) (a) Schoehn, G.; Vellieux, F. M. D.; Dura, M. A.; Receveur-Brechot, V.; Fabry, C. M. S.; Ruigrok, R. W. H.; Ebel, C.; Roussel, A.; Franzetti, B. *J. Biol. Chem.* **2006**, *281*, 36327. (b) Hadler, K. S.; Mitic, N.; Hsu-Chen Yip, S.; Gahan, L. R.; Ollis, D. L.; Schenk, G.; Larrabee, J. A. *Inorg. Chem.* **2010**, *49*, 2727−2734. (c) Jackson, J.; Foo, J.-L.; Tokuriki, N.; Afriat, L.; Carr, P. D.; Kim, H.-K.; Schenk, G.; Tawfik, D. S.; Ollis, D. L. *Proc. Natl. Acad. Sci. U.S.A.* **2009**, *106*, 21631. (d) Larrabee, J. A.; Baumann, T. F.; Cibhisdes, S. J.; Lyons, T. J. *Inorg. Chem.* **1992**, *31*, 3630. (e) Larrabee, J. A.; Leung, C. H.; Moore, R. L.; Thamrong-Nawasawat, T.; Wessler., B. S. H. *J. Am. Chem. Soc.* **2004**, *126*, 12316. (f) Johansson, F. B.; Bond, A. D.; Gro Nielsen, U.; Moubaraki, B.; Murray, K. S.; Berry, K. J.; Larrabee, J. A.; McKenzie, C. J. *Inorg. Chem.* **2008**, *47*, 5079−5092. (g) Strater, N.; Lipscomb, W. N. *Biochemistry* **1995**, *34*, 9200.

(2) (a) Holz, R. C. *Coord. Chem. Rev.* **2002**, *232*, 5. (b) Sommerhalter, M.; Lieberman, R. L.; Rosenzweig, A. C. *Inorg. Chem.* **2005**, *44*, 770−778.

(3) Zhang, J.-H.; Kurtz, D. M., Jr. *Proc. Natl. Acad. Sci. U.S.A.* **1992**, *89*, 7065−7069.

(4) (a) Bennett, B.; Holz, R. C. *J. Am. Chem. Soc.* **1997**, *119*, 1923−1933. (b) Larrabee, J. A.; Alessi, C. M.; Asiedu, E. T.; Cook, J. O.; Hoerning, K. R.; Klingler, L. J.; Okin, G. S.; Santee, S. G.; Volkert, T. L. *J. Am. Chem. Soc.* **1997**, *119*, 4182−4196.

(5) (a) Krzystek, J.; Zvyagin, S. A.; Ozarowski, A.; Fiedler, A. T.; Brunold, T. C.; Telser, J. *J. Am. Chem. Soc.* **2004**, *126*, 2148. (b) Neese, F.; Solomon, E. I. *Inorg. Chem.* **1999**, *38*, 1847.

(6) Coleman, J. E.; Coleman, R. V. *J. Biol. Chem.* **1972**, *247*, 4718.

(7) Werth, M. T.; Tang, S.-F.; Formicka, G.; Zeppezauer, M.; Johnson, M. K. *Inorg. Chem.* **1995**, *34*, 218.

(8) Brader, M. I.; Kaarsholm, N. C.; Harnung, S. E.; Dunn, M. F. *J. Biol. Chem.* **1997**, *272*, 1088.

(9) Suzuki, S.; Hirose, S.; Sawade, S.; Nakahara, N. *Inorg. Chem. Acta* **1985**, *108*, 155.

(10) Hüber, M.; Bubacco, L.; Beltramini, M.; Salvato, B.; Elias, H.; Peisach, J.; Larsen, E.; Harnung, S. E.; Haase, W. *Inorg. Chem.* **1996**, *35*, 7482.

(11) Larrabee, J. A.; Johnson, W. R.; Volwiler, A. S. *Inorg. Chem.* **2009**, *48*, 8822−8829.

(12) Yamami, M.; Tanaka, M.; Sakiyama, H.; Koga, T.; Kobayashi, K.; Miyasaka, H.; Ohba, M.; Okawa, H. *J. Chem. Soc., Dalton Trans.* **1997**, 4595−4601.

(13) Turpeinen, U.; Hämäläinen, R.; Reedijk, J. *Polyhedron* **1987**, *6*, 1603−1610.

(14) Fabelo, O.; Cañadillas-Delgado, L.; Pasán, J.; Delgado, F. S.; Lloret, F.; Cano, J.; Julve, M.; Ruiz-Pérez, C. *Inorg. Chem.* **2009**, *48*, 11342−11351.

(15) Jia, Q.-X.; Tian, H.; Zhang, J.-Y.; Gao, E.-Q. *Chem.—Eur. J.* **2011**, *17*, 1040−1051.

(16) Calvo-Perez, V.; Ostrovsky, S.; Vega, A.; Pelikan, J.; Spodine, E.; Haase, W. *Inorg. Chem.* **2006**, *45*, 644−649.

(17) Aromí, G.; Batsanov, A. S.; Christian, P.; Helliwell, M.; Parkin, A.; Parsons, S.; Smith, A. A.; Timco, G. A.; Winpenny, R. E. P. *Chem.—Eur. J.* **2003**, *9*, 5142−5161.

(18) *CrysAlisRED*, version 1.171.26; Oxford Diffraction Ltd.: Köln, Germany, 2004.

(19) Sheldrick, G. M. *SHELXS-97*; University of Göttingen: Göttingen, Germany, 1997.

(20) Sheldrick, G. M. *SHELXL-97-2*; University of Göttingen: Göttingen, Germany, 1997.

(21) PDB refcode 1MAT solved at 2.40 Å; refcode 2B3H solved at 1.1 Å resolution.

(22) (a) Brown, D. A.; Errington, W.; Glass, W. K.; Haase, W.; Kemp, T. J.; Nimir, H.; Ostrovsky, S. M.; Werner, R. *Inorg. Chem.* **2001**, *40*, 5962−5971. (b) Brown, D. A.; Glass, W. K.; Fitzpatrick, N. J.; Kemp, T. J.; Errington, W.; Clarkson, G. J.; Haase, W.; Falk, K.; Mahdy, A. H. *Inorg. Chim. Acta* **2004**, *357*, 1411−1436.

(23) Ostrovsky, S.; Tomkowicz, Z.; Haase, W. *Coord. Chem. Rev.* **2009**, *253*, 2363.

(24) Lines, M. E. *J. Chem. Phys.* **1971**, *55*, 2977.

(25) Tomkowicz, Z.; Ostrovsky, S.; Mueller-Bunz, H.; Hussein Eltmimi, A. J.; Rams, M.; Brown, D. A.; Haase, W. *Inorg. Chem.* **2008**, *47*, 6956.

(26) Harding, M. J.; Briat, B. *Mol. Phys.* **1973**, *25*, 745.

(27) Beghidja, A.; Rabu, P.; Rogez, G.; Welter., R. *Chem.—Eur. J.* **2006**, *12*, 7627−7638.

(28) Ostrovsky, S. M.; Falk, K.; Pelikan, J.; Brown, D. A.; Tomkowicz, Z.; Haase, W. *Inorg. Chem.* **2006**, *45*, 688.

(29) Ostrovsky, S. M. *Chem. Phys.* **2011**, *386*, 95.

(30) Oganesyan, V. S.; George, S. J.; Cheesman, M. R.; Thomson, A. J. *J. Chem. Phys.* **1999**, *110*, 762.

(31) Kanamori, J. *J. Phys. Chem. Solids* **1959**, *10*, 87.

(32) Kahn, O. *Molecular Magnetism*; VCH Publishers: New York, 1993.

(33) Schultz, B. E.; Ye, B.-H.; Li, X.-y.; Chan, S. I. *Inorg. Chem.* **1997**, *36*, 2617−2622.

(34) Albores, P.; Rentschler, E. *Dalton Trans.* **2009**, 2609−2615.